# MULTI-SCALE HIGHER ORDER SINGULAR VALUE DECOMPOSITION (MS-HOSVD) FOR RESTING-STATE FMRI COMPRESSION AND ANALYSIS

*Alp Ozdemir*[1], *Marisel Villafañe-Delgado*[1], *David C. Zhu*[2], *Mark A. Iwen*[1,3] *and Selin Aviyente*[1]

[1]Department of Electrical and Computer Engineering, Michigan State University
[2]Department of Radiology, Michigan State University
[3]Department of Mathematics, Michigan State University

## ABSTRACT

Advances in information technology are making it possible to collect increasingly massive amounts of multidimensional, multi-modal neuroimaging data such as functional magnetic resonance imaging (fMRI). Current fMRI datasets involve multiple variables including multiple subjects, as well as both temporal and spatial data. These high dimensional datasets pose a challenge to the signal processing community to develop data reduction methods that can exploit their rich structure and extract meaningful summarizations. In this paper, we propose a tensor-based framework for data reduction and low-dimensional structure learning with a particular focus on reducing high dimensional fMRI data sets into physiologically meaningful network components. We develop a multiscale tensor factorization method for higher order data inspired by hybrid linear modeling and subspace clustering techniques. In particular, we develop a multi-scale HoSVD approach where a given tensor is first permuted and then partitioned into several sub-tensors each of which can be represented more efficiently. This multi-scale framework is applied to resting state fMRI data to identify the default mode network from compressed data.

***Index Terms***— Higher Order SVD, resting state fMRI, tensor

## 1. INTRODUCTION

Human brain is a complex network of functionally and structurally interconnected regions. The advance in neuroimaging technology has led to incredible amount of digital data that can be used to study this complex network. This includes data from multiple subjects, multiple imaging modalities, e.g., structural versus functional, and multiple experimental conditions, e.g. in action or rest. Along with advances in the ability to obtain data, there has been an increase in the numbers of multisite consortia for examining the healthy and diseased brain [1, 2]. Most of this data is shared openly with the data science community through platforms such as "1000 Functional Connectomes" project, OpenfMRI and Human Brain Mapping Initiative [3]. As such neuroimaging provides an attractive application site for data scientists to reduce, analyze and interpret these large amounts of imaging data.

One particular application of interest is the study of functional connectivity networks from neuroimaging data. Resting-state functional connectivity magnetic resonance imaging (fcMRI) studies constitute a growing proportion of functional brain imaging literature [4, 5]. This approach detects temporal correlations in spontaneous blood oxygen level-dependent (BOLD) signal oscillations of widely separated brain regions while subjects rest quietly in the scanner. Biswal et al. [6] were the first to demonstrate meaningful connectivity networks between the left and right hemispheric regions of the primary motor network, suggesting ongoing information processing between these regions even when the subjects were not actively involved in a task. Several methods to process resting-state fMRI data have been proposed including seed methods [6], principal component analysis (PCA) [7], singular value decomposition, independent component analysis (ICA) [8, 9] and clustering [10]. The different methods have reported similar resting-state networks, including the motor network, the visual network, two lateralized networks consisting of superior parietal and superior frontal regions and the default mode network (DMN) consisting of precuneus, medial frontal and inferior parietal and temporal regions [11, 12]. DMN is detectable using task-free fMRI and consists of a set of brain regions that typically deactivate during performance of cognitive tasks suggesting that activity of this network is reflecting a default state of neuronal activity of the human brain [13].

With the availability of big neuroimaging datasets, in particular resting state fMRI data, it is important to be able to extract meaningful network components, such as the DMN, from compressed data with reasonable computational efficiency. The early work on fMRI data compression focused on adapting well-known lossless video compression algorithms such as SPIHT and H.264 [14, 15, 16]. However, the

This work was in part supported by NSF CCF-1422262 and CCF-1615489.

performance of these algorithms were solely evaluated based on the compression ratio achieved without any attention to the reproducibility of the network components extracted from the original data. In recent years, tensors have been proposed as a plausible tool to represent and analyze fMRI data and the corresponding networks [17, 18]. However, the work in this area has been limited to extending linear, low-rank matrix methods such as ICA and SVD to the tensor case and has not considered the use of tensors and tensor decompositions for fMRI data reduction and compression. Therefore, these low-rank approximations obtained by such linear methods may not efficiently encode the data points belonging to nonlinear manifolds [19, 20].

In this paper, we propose a new tensor based framework for data reduction with a particular focus on reducing resting state fMRI datasets. This multiresoultion analysis framework aims to efficiently encode nonlinearities in tensor type data. The proposed method is inspired by geometric multiresolution analysis (GMRA) [19] and its multiscale structure. Similar to GMRA, the proposed method constructs data-dependent multiscale dictionaries to better represent the data. The proposed algorithm consists of two main steps: 1) Constructing a tree structure by decomposing the tensor into a collection of permuted subtensors, and 2) Constructing multiscale dictionaries by applying higher order SVD (HoSVD) to each subtensor. Finally, we apply the proposed algorithm to rfMRI datasets and evaluate the success of recovering DMNs from the compressed data with respect to the original data and compare the improvement in the compression performance with respect to regular HoSVD.

## 2. RELATION TO PRIOR WORK

This paper has two major contributions. First, we propose a new way to decompose generic tensors. Recently, various tensor decomposition techniques including hierarchical Tucker decomposition and tensor train decomposition have been proposed to reduce the memory requirements of Tucker decomposition for big tensors [21, 22]. However, these tensor decomposition techniques do not consider efficient encoding of data points sampled from nonlinear manifolds. In this paper, we propose a new multiscale tensor decomposition which better approximates nonlinearities in a tensor. Second, we propose a new compression framework for fMRI datasets. Recent studies on fMRI data compression depend on well-known lossless video and image compression algorithms without any particular attention to the structure of the fMRI volume data [14, 15, 16]. However, in this study, we consider multilinear local structure of tensor type data and propose a tensor based approach to compress fMRI datasets.

## 3. MULTISCALE TENSOR DECOMPOSITION

In this section, we present a multiscale analysis procedure named as Multiscale HoSVD (MS-HoSVD) for an $N$th order tensor $\mathscr{X} \in \mathbb{R}^{I_1 \times I_2 \times \ldots \times I_N}$. The proposed method recursively applies the following two-step approach: (i) Low-rank tensor approximation, (ii) Decomposing the residual (original minus low-rank) tensor into subtensors.

A tensor $\mathscr{X}$ is decomposed using HoSVD as follows:

$$\mathscr{X} = \mathscr{C} \times_1 \mathbf{U}^{(1)} \times_2 \mathbf{U}^{(2)} \ldots \times_N \mathbf{U}^{(N)}, \tag{1}$$

where $\mathbf{U}^{(n)}$s are the mode matrices containing the left singular vectors of $\mathbf{X}_{(n)}$s obtained by unfolding $\mathscr{X}$ along $n$th mode. The low-rank approximation of $\mathscr{X}$ is obtained by

$$\hat{\mathscr{X}_0} = \mathscr{C}_0 \times_1 \hat{\mathbf{U}}^{(1)} \times_2 \hat{\mathbf{U}}^{(2)} \ldots \times_N \hat{\mathbf{U}}^{(N)}, \tag{2}$$

where $\hat{\mathbf{U}}^{(n)}$s are the truncated mode matrices obtained by keeping the first $r_n$ columns of $\mathbf{U}^{(n)}$ and $\mathscr{C}_0 = \mathscr{X} \times_1 \hat{\mathbf{U}}^{(1),\top} \times_2 \hat{\mathbf{U}}^{(2),\top} \ldots \times_N \hat{\mathbf{U}}^{(N),\top}$. The tensor $\mathscr{X}$ can now be written as

$$\mathscr{X} = \hat{\mathscr{X}_0} + \mathscr{W}_0, \tag{3}$$

where $\mathscr{W}_0$ is the residual tensor.

In this paper, we focus on a single scale analysis even though the extension to multiple scales follows directly. The residual tensor of 0th scale $\mathscr{W}_0$ is first decomposed into subtensors as follows. Tensor $\mathscr{W}_0 \in \mathbb{R}^{I_1 \times I_2 \times \ldots \times I_N}$ is unfolded across each mode yielding $\mathbf{W}_{0,(n)} \in \mathbb{R}^{I_n \times \prod_{j \neq n} I_j}$ whose columns are the mode-$n$ fibers of $\mathscr{W}_0$. For each mode, rows of $\mathbf{W}_{0,(n)}$ are partitioned into $c_n$ non-overlapping clusters by a clustering algorithm and the Cartesian product of the partitioning labels coming from different modes yields index sets of $K = \prod_{i=1}^{N} c_i$ subtensors $\mathscr{X}_{1,k}$ where $k \in \{1, 2, \ldots, K\}$.

Let $J_0^n$ be the index set corresponding to the $n$th mode of $\mathscr{W}_0$ where $J_0^n = \{1, 2, \ldots, I_n\}$, $J_{1,k}^n$ be the index set of the subtensor $\mathscr{X}_{1,k}$ for the $n$th mode, where $J_{1,k}^n \subset J_0^n$ with $n \in \{1, 2, \ldots N\}$. Index sets of subtensors satisfy $\cup_{k=1}^{K} J_{1,k}^n = J_0^n$ and $J_{1,k}^n \cap J_{1,l}^n = \emptyset$ when $k \neq l$ for all $k$, $l \in \{1, 2, \ldots, K\}$. For example, the index set of the first subtensor $\mathscr{X}_{1,1}$ can be written as $J_{1,1}^1 \times J_{1,1}^2 \times \ldots \times J_{1,1}^N$ and the $k$th subtensor $\mathscr{X}_{1,k}$ is obtained by

$$\begin{gathered} \mathscr{X}_{1,k}(i_1, i_2, \ldots, i_N) = \mathscr{W}_0(J_{1,k}^1(i_1), J_{1,k}^2(i_2), \ldots, J_{1,k}^N(i_N)), \\ \mathscr{X}_{1,k} = \mathscr{W}_0(J_{1,k}^1 \times J_{1,k}^2 \times \ldots \times J_{1,k}^N), \end{gathered} \tag{4}$$

where $i_n \in \left\{1, 2, \ldots, J_{1,k}^n\right\}$. To increase efficiency, subtensors whose energy is below a certain threshold can be removed from the multiscale structure. Then, low-rank approximation for each subtensor is obtained by applying HoSVD as:

$$\hat{\mathscr{X}_{1,k}} = \mathscr{C}_{1,k} \times_1 \hat{\mathbf{U}}_{1,k}^{(1)} \times_2 \hat{\mathbf{U}}_{1,k}^{(2)} \ldots \times_N \hat{\mathbf{U}}_{1,k}^{(N)}, \tag{5}$$

where $\mathscr{C}_{1,k}$ and $\hat{\mathbf{U}}_{1,k}^{(n)}$s correspond to the core tensor and low-rank projection matrices of $\mathscr{X}_{1,k}$, respectively. $\hat{\mathscr{X}_1}$ is the 1st

scale approximation of $\mathscr{X}$ formed by mapping all of the subtensors onto $\hat{\mathscr{X}}_1$ as follows:

$$\hat{\mathscr{X}}_1(J^1_{1,k} \times J^2_{1,k} \times ... \times J^n_{1,k}) = \hat{\mathscr{X}}_{1,k}. \quad (6)$$

Similarly 1st scale residual tensor is obtained by

$$\mathscr{W}_1(J^1_{1,k} \times J^2_{1,k} \times ... \times J^n_{1,k}) = \mathscr{W}_{1,k}, \quad (7)$$

where $\mathscr{W}_{1,k} = \mathscr{X}_{1,k} - \hat{\mathscr{X}}_{1,k}$. Therefore $\mathscr{X}$ can be rewritten as:

$$\mathscr{X} = \hat{\mathscr{X}}_0 + \mathscr{W}_0 = \hat{\mathscr{X}}_0 + \hat{\mathscr{X}}_1 + \mathscr{W}_1. \quad (8)$$

The $j$th scale approximation of $\mathscr{X}$ is obtained by decomposing $\mathscr{W}_{j-1,k}$s into subtensors $\mathscr{X}_{j,k}$s and fitting low-rank model to each one of them. Finally, $\mathscr{X}$ can be written as:

$$\mathscr{X} = \sum_{i=0}^{n} \hat{\mathscr{X}}_i + \mathscr{W}_n. \quad (9)$$

A pseudo code of the MS-HoSVD with 1-scale approximation is given in Algorithm 1.

**Algorithm 1** Multiscale HoSVD with 1-Scale Analysis

Input: $\mathscr{X}$: tensor , $\mathbf{C} = (c_1, c_2, ..., c_N)$: the desired number of clusters for each mode.
Output: $\hat{\mathscr{X}}$: 1-scale low-rank approximation of $\mathscr{X}$, $T$: Tree structure containing the MS-HoSVD decomposition of $\mathscr{X}$.
Create an empty tree $T$.
$\mathscr{C}_0, \left\{\hat{\mathbf{U}}^{(1)}, ..., \hat{\mathbf{U}}^{(N)}\right\} \leftarrow$ truncatedHOSVD($\mathscr{X}$).
$\hat{\mathscr{X}}_0 = \mathscr{C}_0 \times_1 \hat{\mathbf{U}}^{(1)} \times_2 \hat{\mathbf{U}}^{(2)} ... \times_N \hat{\mathbf{U}}^{(N)}$.
$\mathscr{W}_0 \leftarrow \mathscr{X} - \hat{\mathscr{X}}_0$.
Add root node to the tree $T$ containing $\mathscr{C}_0$ and $\hat{\mathbf{U}}^{(i)}$s where $i \in \{1, 2, ...N\}$.
Create subtensors $\mathscr{X}_{1,k}$ and index sets $J^n_{1,k}$ from $\mathscr{W}_0$ where $k \in \{1, 2, ..., K\}$, $n \in \{1, 2, ..., N\}$ and $K = \prod_{n=1}^{N} c_n$.
**for** k = 1 to K **do**
  **if** $\frac{\| \mathscr{X}_{1,k} \|}{\prod_{n=1}^{N} |J^n_{1,k}|} \geq 0.01 \frac{\| \mathscr{X} \|}{\prod_{n=1}^{N} I_n}$ **then**
    $\mathscr{C}_{1,k}, \left\{\hat{\mathbf{U}}^{(1)_{1,k}}, ..., \hat{\mathbf{U}}^{(N)}_{1,k}\right\} \leftarrow$ truncatedHOSVD($\mathscr{X}_{1,k}$).
    Add the node containing $\mathscr{C}_{1,k}$, $\left\{\hat{\mathbf{U}}^{(1)}_{1,k}, ..., \hat{\mathbf{U}}^{(N)}_{1,k}\right\}$ and $\left\{J^1_{1,k}, ..., J^N_{1,k}\right\}$ to the tree $T$.
    $\hat{\mathscr{X}}_1(J^1_{1,k} \times J^2_{1,k} \times ... \times J^n_{1,k}) = \hat{\mathscr{X}}_{1,k}$.
  **end if**
**end for**
$\hat{\mathscr{X}} = \hat{\mathscr{X}}_0 + \hat{\mathscr{X}}_1$.

## 4. DATA DESCRIPTION AND PREPROCESSING

The data used in this paper is obtained from 1000 Functional Connectomes Project [23] (`http://www.nitrc.org/projects/fcon_1000`) which has aggregated previously collected test-retest imaging datasets from more than 36 labs around the world. The data acquired from above url is referred to as Bangor which contains open-eye resting state fMRI scans of 20 male participants aged between 19-38 (Magnet: 3T, TR = 2, 34 slices, 265 time points).

The data were pre-processed using CONN functional connectivity toolbox [24]. First, structural images were co-registered to the mean functional image for each subject and normalized to MNI space. Then, slice timing correction and motion correction were performed for each functional images. The functional images were warped to Talairach Daemon atlas [25] provided by CONN toolbox and smoothed with an 4-mm FWHM Gaussian kernel. Confounds such as motion parameters obtained from reallignment and bold signals obtained from white matter and CSF masks were regressed out and band-pass (0.008-0.09 Hz) temporal filtering was applied to functional images of each subject. After pre-processing, the fMRI dataset can be represented as a 4-mode tensor $\mathscr{X}^m \in \mathbb{R}^{109 \times 91 \times 91 \times 265}$ for each subject $m \in \{1, 2, ..., 20\}$ where the first three modes correspond to the preprocessed volume data and the fourth mode to time.

## 5. RESULTS

In this section, we evaluated the performance of the MS-HoSVD in comparison to HoSVD for both compression and error rate. $\mathscr{X}^m$s obtained from preprocessing are decomposed by using MS-HoSVD yielding $\hat{\mathscr{X}}^m_{MS}$ and HoSVD $\hat{\mathscr{X}}^m_{HO}$, respectively. In the following experiments, clustering is performed by by local subspace analysis (LSA) [26] and the number of clusters along each mode is chosen as $c_i = 4$. The rank used in truncated HoSVD is selected adaptively depending on the energy criterion. Energy criterion determines the minimum number of singular values kept during the SVD of the unfolded tensors along each mode such that the cumulative energy is above a certain threshold. For MS-HoSVD, the energy thresholds are selected as 0.7 and 0.95 for the SVDs computed for 0th and 1st scales, respectively. For Ho-SVD, the energy threshold increased gradually from 0.990 to 0.999 with a step size of 0.0005 to compare the reconstruction error at similar compression ratios (experiment-1) and the compression rate for the similar error rates (experiment-2). In Table 1 the error rate refers to the normalized tensor approximation error $\frac{\|\mathscr{X} - \hat{\mathscr{X}}\|_F}{\|\mathscr{X}\|_F}$ and the compression ratio is computed as $\frac{\text{\# total bits to store } \mathscr{X}}{\text{\# total bits to store } \hat{\mathscr{X}}}$. As seen in Table, 1, MS-HoSVD provides reduced error (experiment-1) and better compression than HoSVD (expermient-2) for 20 subjects.

Once low-rank approximations are obtained, mean ROI signals $\mathbf{Y}^m \in \mathbb{R}^{88 \times 265}$, $\mathbf{Y}^m_{MS} \in \mathbb{R}^{88 \times 265}$ and $\mathbf{Y}^m_{HO} \in \mathbb{R}^{88 \times 265}$ corresponding to $\mathscr{X}^m$, $\hat{\mathscr{X}}^m_{MS}$ and $\hat{\mathscr{X}}^m_{HO}$ are computed for each subject using Talairach Daemon atlas. Connectivity networks for each subject $m$ are denoted as $\mathbf{A}^m \in \mathbb{R}^{88 \times 88}$, $\mathbf{A}^m_{HO} \in \mathbb{R}^{88 \times 88}$, $\mathbf{A}^m_{MS} \in \mathbb{R}^{88 \times 88}$, and are constructed by computing the correlation coefficient between all ROIs in $\mathbf{Y}^m$,

**Table 1**. Average compression ratio (mean±st.dev) and reconstruction error (mean±st.dev) obtained by MS-HoSVD and HoSVD over 20 subjects.

| | MS-HoSVD | HoSVD (Exp-1) | HoSVD (Exp-2) |
|---|---|---|---|
| Comp. Ratio | 10.3275±0.6287 | 10.3736±0.5955 | 8.3068±0.6427 |
| Rec. Error | 0.0231±0.0018 | 0.0404±0.0061 | 0.0228±0.0040 |

$\mathbf{Y}^m_{MS}$ and $\mathbf{Y}^m_{HO}$, respectively. Significant connections ($p \leq 0.01$, Bonferroni corrected) for each method were determined by performing t-tests for each edge of connectivity matrices over subjects. Table 2 shows the miss and false alarm rates for the connectivity networks constructed using MS-HoSVD and HoSVD in comparison to the original network. As it can be seen from Table 2, we obtain lower error rates for MS-HoSVD compared to HoSVD for both experiments.

**Table 2**. Comparisons of probability of miss ($P_{Miss}$) and probability of false alarm ($P_{FA}$) obtained by MS-HoSVD and HoSVD.

| | MS-HoSVD | HoSVD (Exp-1) | HoSVD (Exp-2) |
|---|---|---|---|
| $P_{Miss}$ | 0.0020 | 0.0033 | 0.0031 |
| $P_{FA}$ | 0 | 0.0006 | 0 |

Fig.1 illustrates the DMN extracted from MS-HoSVD based on the statistically significant pairwise correlation between all pairs of following ROIs: left and right superior frontal gyri (SFG), medial frontal cortex (MFC), anterior cingulate cortex (ACC), posterior cingulate cortex (PCC), left and right angular gyri (AG), and left and right hippocampus. As seen in Fig.1, there is strong connectivity between core regions in the DMN, as the PCC, MeFC and ACC. DMNs extracted from the original data and the compressed were indistinguishable from each other indicating that even at a compression ratio of 10:1 we can still detect the significant network components without any error.

## 6. CONCLUSIONS

In this paper, we introduced a new tensor decomposition technique for better compression of higher order fMRI tensors using the local nonlinearities in the data. The proposed approach constructs a tree structure by clustering the tensor across its modes and then decomposes the tensor into lower dimensional subtensors. A low-rank approximation of each subtensor is then obtained by HoSVD. The proposed approach is applied to 4th order fMRI tensors and the connectivity networks obtained from the compressed data are compared to the original networks.

Future work will consider the extension of this approach to higher order tensors, by including the different subjects as another mode as well as to multiple scales. In this manner, it would be possible to obtain a joint compression at the group level for multiple subjects thus obtaining higher compression ratios. Future work will also focus on fast implementation of the proposed approach through parallel construction of subtensors and paralel implementation of HoSVD.

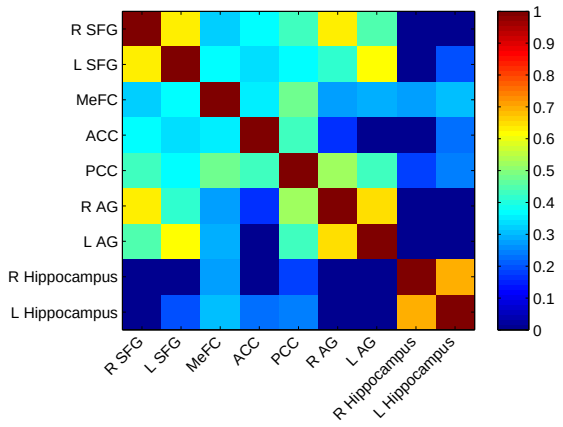


**Fig. 1**. Default mode network obtained from MS-HoSVD.

## 7. REFERENCES


[1] Russell A Poldrack and Krzysztof J Gorgolewski, "Making big data open: data sharing in neuroimaging," *Nature neuroscience*, vol. 17, no. 11, pp. 1510–1517, 2014.

[2] Xi-Nian Zuo, Jeffrey S Anderson, Pierre Bellec, Rasmus M Birn, Bharat B Biswal, Janusch Blautzik, John CS Breitner, Randy L Buckner, Vince D Calhoun, F Xavier Castellanos, et al., "An open science resource for establishing reliability and reproducibility in functional connectomics," *Scientific data*, vol. 1, pp. 140049, 2014.

[3] John Darrell Van Horn and Arthur W Toga, "Human neuroimaging as a big data science," *Brain imaging and behavior*, vol. 8, no. 2, pp. 323–331, 2014.

[4] Martijn P Van Den Heuvel and Hilleke E Hulshoff Pol, "Exploring the brain network: a review on resting-state fmri functional connectivity," *European Neuropsychopharmacology*, vol. 20, no. 8, pp. 519–534, 2010.

[5] Michael D Greicius, Kaustubh Supekar, Vinod Menon, and Robert F Dougherty, "Resting-state functional connectivity reflects structural connectivity in the default mode network," *Cerebral cortex*, vol. 19, no. 1, pp. 72–78, 2009.

[6] Bharat Biswal, F Zerrin Yetkin, Victor M Haughton, and James S Hyde, "Functional connectivity in the motor cortex of resting human brain using echo-planar mri," *Magnetic resonance in medicine*, vol. 34, no. 4, pp. 537–541, 1995.

[7] Felix Carbonell, Pierre Bellec, and Amir Shmuel, "Global and system-specific resting-state fmri fluctuations are uncorrelated: principal component analysis reveals anti-correlated networks," *Brain connectivity*, vol. 1, no. 6, pp. 496–510, 2011.

[8] Madiha J Jafri, Godfrey D Pearlson, Michael Stevens, and Vince D Calhoun, "A method for functional network connectivity among spatially independent resting-state components in schizophrenia," *Neuroimage*, vol. 39, no. 4, pp. 1666–1681, 2008.

[9] Christian F Beckmann, Marilena DeLuca, Joseph T Devlin, and Stephen M Smith, "Investigations into resting-state connectivity using independent component analysis," *Philosophical Transactions of the Royal Society of London B: Biological Sciences*, vol. 360, no. 1457, pp. 1001–1013, 2005.

[10] Martijn Van Den Heuvel, Rene Mandl, and Hilleke Hulshoff Pol, "Normalized cut group clustering of resting-state fmri data," *PloS one*, vol. 3, no. 4, pp. e2001, 2008.

[11] Michael D Greicius, Ben Krasnow, Allan L Reiss, and Vinod Menon, "Functional connectivity in the resting brain: a network analysis of the default mode hypothesis," *Proceedings of the National Academy of Sciences*, vol. 100, no. 1, pp. 253–258, 2003.

[12] Michael D Fox and Marcus E Raichle, "Spontaneous fluctuations in brain activity observed with functional magnetic resonance imaging," *Nature Reviews Neuroscience*, vol. 8, no. 9, pp. 700–711, 2007.

[13] Marcus E Raichle, Ann Mary MacLeod, Abraham Z Snyder, William J Powers, Debra A Gusnard, and Gordon L Shulman, "A default mode of brain function," *Proceedings of the National Academy of Sciences*, vol. 98, no. 2, pp. 676–682, 2001.

[14] Hariharan G Lalgudi, Ali Bilgin, Michael W Marcellin, and Mariappan S Nadar, "Compression of fmri and ultrasound images using 4d spiht," in *IEEE International Conference on Image Processing 2005*. IEEE, 2005, vol. 2, pp. II–746.

[15] Victor Sanchez, Panos Nasiopoulos, and Rafeef Abugharbieh, "Novel lossless fmri image compression based on motion compensation and customized entropy coding," *IEEE Transactions on Information Technology in Biomedicine*, vol. 13, no. 4, pp. 645–655, 2009.

[16] Fabian J Theis and Toshihisa Tanaka, "A fast and efficient method for compressing fmri data sets," in *International Conference on Artificial Neural Networks*. Springer, 2005, pp. 769–777.

[17] Christian F Beckmann and Stephen M Smith, "Tensorial extensions of independent component analysis for multisubject fmri analysis," *Neuroimage*, vol. 25, no. 1, pp. 294–311, 2005.

[18] Ian Davidson, Sean Gilpin, Owen Carmichael, and Peter Walker, "Network discovery via constrained tensor analysis of fmri data," in *Proceedings of the 19th ACM SIGKDD international conference on Knowledge discovery and data mining*. ACM, 2013, pp. 194–202.

[19] William K Allard, Guangliang Chen, and Mauro Maggioni, "Multi-scale geometric methods for data sets ii: Geometric multi-resolution analysis," *Applied and Computational Harmonic Analysis*, vol. 32, no. 3, pp. 435–462, 2012.

[20] Zhenyue Zhang, Jing Wang, and Hongyuan Zha, "Adaptive manifold learning," *Pattern Analysis and Machine Intelligence, IEEE Transactions on*, vol. 34, no. 2, pp. 253–265, 2012.

[21] Lars Grasedyck, "Hierarchical singular value decomposition of tensors," *SIAM Journal on Matrix Analysis and Applications*, vol. 31, no. 4, pp. 2029–2054, 2010.

[22] Ivan V Oseledets, "Tensor-train decomposition," *SIAM Journal on Scientific Computing*, vol. 33, no. 5, pp. 2295–2317, 2011.

[23] Bharat B Biswal, Maarten Mennes, Xi-Nian Zuo, Suril Gohel, Clare Kelly, Steve M Smith, Christian F Beckmann, Jonathan S Adelstein, Randy L Buckner, Stan Colcombe, et al., "Toward discovery science of human brain function," *Proceedings of the National Academy of Sciences*, vol. 107, no. 10, pp. 4734–4739, 2010.

[24] Susan Whitfield-Gabrieli and Alfonso Nieto-Castanon, "Conn: a functional connectivity toolbox for correlated and anticorrelated brain networks," *Brain connectivity*, vol. 2, no. 3, pp. 125–141, 2012.

[25] Jack L Lancaster, Marty G Woldorff, Lawrence M Parsons, Mario Liotti, Catarina S Freitas, Lacy Rainey, Peter V Kochunov, Dan Nickerson, Shawn A Mikiten, and Peter T Fox, "Automated talairach atlas labels for functional brain mapping," *Human brain mapping*, vol. 10, no. 3, pp. 120–131, 2000.

[26] Jingyu Yan and Marc Pollefeys, "A general framework for motion segmentation: Independent, articulated, rigid, non-rigid, degenerate and non-degenerate," in *Computer Vision–ECCV 2006*, pp. 94–106. Springer, 2006.